Correlation of shape and magnetic anisotropy of supported mass-filtered Fe and FeCo alloy nanoparticles on W(110)

2008 J. Phys.: Condens. Matter 20 445005

(http://iopscience.iop.org/0953-8984/20/44/445005)

J. Phys.: Condens. Matter **20** (2008) 445005 (6pp) doi:10.1088/0953-8984/20/44/445005

Correlation of shape and magnetic anisotropy of supported mass-filtered Fe and FeCo alloy nanoparticles on W(110)

A Kleibert[1], F Bulut[2,3], R K Gebhardt[2], W Rosellen[2], D Sudfeld[4], J Passig[1], J Bansmann[3], K H Meiwes-Broer[1] and M Getzlaff[2]

[1] Institut für Physik, Universität Rostock, Universitätsplatz 3, D-18051 Rostock, Germany
[2] Institut für Angewandte Physik, Universität Düsseldorf, Universitätsstrasse 1, D-40225 Düsseldorf, Germany
[3] Institut für Oberflächenchemie und Katalyse, Universität Ulm, Albert-Einstein-Allee 47, D-89069 Ulm, Germany
[4] Institut für Experimentalphysik, Universität Duisburg-Essen, Lotharstrasse 1, D-47048 Duisburg, Germany

E-mail: getzlaff@uni-duesseldorf.de

Received 29 July 2008, in final form 2 September 2008
Published 25 September 2008
Online at stacks.iop.org/JPhysCM/20/445005

Abstract

Mass-filtered Fe and FeCo nanoparticles are deposited under soft-landing and ultra-high vacuum conditions on the bare W(110) surface. The structure and the stoichiometry of FeCo alloy nanoparticles are determined by *ex situ* high resolution transmission electron microscopy (HRTEM) and energy-dispersive x-ray spectroscopy (EDX) on single nanoparticles, respectively, proving a crystalline structure. *In situ* scanning tunneling microscopy (STM) shows that the clusters are irregularly distributed on the W(110) surface, that no fragmentation occurs, that steps do not act as preferential adsorption sites, and yields strong evidence for a partial flattening of the particles upon deposition. The magnetic anisotropy energy (MAE) of mass-filtered pure Fe nanoparticles is investigated by means of x-ray magnetic circular dichroism (XMCD) at the iron L_3 edge. The magnetization loops reveal an uniaxial magnetic anisotropy with the magnetic hard axis being perpendicular to the surface. The experimentally determined MAE is compared to calculated shape and interface anisotropy contributions of partially flattened nanoparticles according to the STM observations on the FeCo clusters.

(Some figures in this article are in colour only in the electronic version)

1. Introduction

Due to their finite size, electronic and magnetic properties of clusters and nanoparticles differ from their respective bulk and thin film materials [1–3]. Enhanced magnetic moments with a non-monotonic dependence on the number of atoms have been observed in Stern–Gerlach experiments on 3d transition metal clusters in the gas phase [4, 5]. When the clusters are supported the nature of the substrate also has a significant impact on their magnetic properties, e.g. the magnetic orbital and spin moments as well as the magnetic anisotropy energy (MAE) [6–9]. When extrapolating these experiments to larger systems, the onset of bulk-like properties might be anticipated at about 1000 atoms per cluster. However, recent investigations revealed that the choice of a particular substrate or capping with metal layers can result in significantly different magnetic properties even for much larger nanoparticles [10–14]. The reported findings basically result from interface and substrate-mediated effects as hybridization of electronic states at the interface, magnetic coupling via surface states and misfit-induced strain, respectively.

Besides the fundamental interest in magnetic phenomena at the nanoscale, supported magnetic nanoparticles are relevant for applications such as, for instance, in future ultra-high density storage devices [15]. These require nanostructures with both a high saturation magnetization for fast reading

and writing of magnetic bits and a sufficiently high MAE in order to overcome the so-called superparamagnetic limit when reducing the size of the storage bits. Materials with a high magneto-crystalline anisotropy energy such as CoPt or FePt alloys have attracted much attention for this purpose in the past [16, 17]. Wet-chemical based techniques are nowadays available to prepare monodispersed arrays of such nanoparticles, but additional treatment is often necessary in order to achieve the desired high MAE phase [18]. More recently, it turned out that tetragonally distorted FeCo may also possess magneto-crystalline anisotropy with comparably high magnitude but significantly larger saturation magnetization [19, 20]. FeCo alloy nanoparticles are therefore highly interesting candidates when developing respective devices.

When preformed nanoparticles are deposited from the gas phase additional degrees of freedom for tuning their magnetic properties become available. Their structure and morphology on the substrate is determined by their size, kinetic energy and the cohesive energies between the clusters and the surface. As a result sizable shape and interface contributions to the total MAE may arise. Also otherwise metastable structures might be stabilized, resulting in properties that are not accessible by other preparation methods. In order to study the complex relation of shape, size and interface on the magnetic properties of deposited nanoparticles, we combine in this contribution scanning tunneling microscopy (STM), high resolution transmission electron microscopy (HRTEM) and magnetic investigations by x-ray magnetic circular dichroism (XMCD). As model systems we have chosen FeCo and Fe nanoparticles on W(110).

This paper is organized as follows. After a brief description of the employed experimental methods and preparation conditions in section 2, we first present results on the structure and the size distribution of FeCo nanoparticles supported by amorphous carbon sheets (i.e. weakly interacting substrates) as determined by means of HRTEM. Particles with the same size are then investigated by means of *in situ* STM after deposition onto a W(110) surface. The measured particle height distribution is compared to the size distribution from the HRTEM images and reveals evidence for partial flattening of the particles on the strongly interacting tungsten substrate. Finally, we show that pure Fe particles supported by W(110) possess a remarkable magnetic anisotropy, most likely due to a partial flattening as observed in the case of the FeCo nanoparticles. This is supported by calculations on the magnetic shape, surface and interface anisotropy contributions to the total MAE of accordingly modeled nanoparticles.

2. Experimental details

All experiments are performed at room temperature under ultra-high vacuum (UHV) conditions in order to avoid any influence by contaminants, particularly oxidation. The base pressures are $p \leqslant 1 \times 10^{-10}$ mbar (STM) and $p \leqslant 1 \times 10^{-9}$ mbar (sample preparation, deposition, XMCD). For the *ex situ* HRTEM and energy-dispersive x-ray analysis studies a FEI Tecnai 20 T with a field-emission gun operating at 200 kV is employed. It yields a point-to-point resolution of 0.24 nm. Energy-dispersive x-ray spectroscopy (EDX) is carried out using the scanning transmission electron microscope (STEM) mode with a spot size being about 1 nm. In these experiments the FeCo nanoparticles are deposited onto commercial TEM grids being covered by amorphous carbon layers. The XMCD investigations on the Fe nanoparticles on W(110) are carried out at the PM 3 beamline of the electron storage ring BESSY (Berlin). Magnetization curves are recorded by means of total electron yield detection at the iron L_3 edge. A magnetic field $\vec{B}$ is applied at variable angles with respect to the sample surface normal allowing us to probe anisotropic magnetic properties as reported in [3]. For detailed information on XMCD, the reader is referred to the literature [21–23]. For the STM experiment we use a commercial MicroSTM (Omicron) working at room temperature in the constant current mode. The probe tips are prepared by chemical etching of a tungsten wire. For both XMCD and STM experiments, the mass-filtered nanoparticles are deposited on a clean W(110) substrate.

The W(110) single-crystal surface is prepared, referring to the common procedure [24], as follows: at an oxygen partial pressure of 1×10^{-6} mbar the crystal is heated at about 1600 K for a prolonged time. At this temperature carbon segregates from the bulk to the surface and oxidizes; the surface region becomes carbon-depleted and passivated by tungsten oxide. To yield a clean and well-ordered surface a 'flash' to 2400 K at a base pressure of $p \leqslant 1 \times 10^{-9}$ mbar is subsequently carried out. Nanoparticle deposits are prepared by means of a continuously working arc cluster ion source (ACIS) which has been described in detail in earlier publications [25–27]. The ACIS is optimized to generate a high flux of mass-filtered metal nanoparticles in the size regime from 4 to 15 nm and is based on an arc discharge in a hollow cathode consisting of the target material. For the present work we use a magnetic alloy (VACOFLUX 50, distributed by Vacuumschmelze GmbH, Germany) with a stoichiometry of $Fe_{50}Co_{48}V_2$ and Fe with a purity of 99%. Due to the arc erosion a high percentage of the nanoparticles is charged, either positively or negatively, allowing a mass separation of the nanoparticles in a static electric field (here, a quadrupole deflector). The deflection voltage of the electrostatic quadrupole U_{quad} can be tuned between 250 V and about 5000 V corresponding to particle sizes between 4 nm and about 15 nm with a resolution of about $\Delta m/m \approx 10\%$ which is sufficient for our purpose. The kinetic energy of the nanoparticles prior to deposition is below the threshold for fragmentation, usually less than 0.1 eV per atom. The complete source including the mass-filtering unit is UHV compatible and thus enables true *in situ* experiments.

3. Results and discussion

3.1. Characterization of FeCo nanoparticles using TEM

Ex situ TEM and HRTEM investigations have been carried out in order to determine the size distribution of nanoparticle deposits. For the present experiments FeCo nanoparticles have been prepared using a quadrupole voltage of $U_{\mathrm{quad}} = 1000$ V. The samples are subsequently transferred under

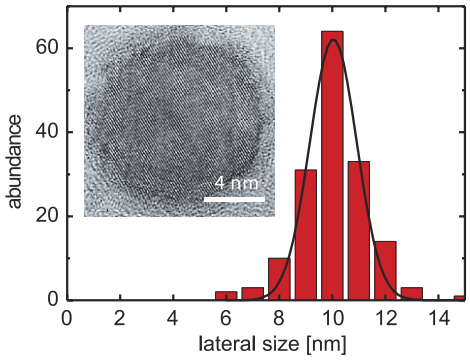

Figure 1. Size distribution of FeCo nanoparticles (deflection voltage $U_{\mathrm{quad}} = 1000$ V) deposited onto a carbon-coated TEM grid, corrected for the influence of oxidation. Solid line: a Gaussian fit yields $D = (10.0 \pm 1.5)$ nm. Inset: HRTEM image of an individual FeCo nanoparticle exhibiting an oxidic shell of about 2 nm resulting in an entire diameter of 15 nm.

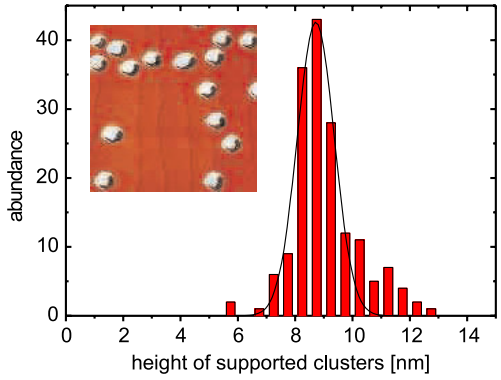

Figure 2. Inset: STM image of FeCo nanoparticles on W(110), 300 nm × 300 nm, $I = 0.1$ nA, $U = +1.0$ V, $U_{\mathrm{quad}} = 1000$ V as in figure 1. Main image: corresponding height distribution of 170 nanoparticles. The height according to the fitted Gaussian amounts to (8.7 ± 1.3) nm.

ambient conditions to the microscope. The resulting formation of a native oxide shell is observed in high resolution TEM images as depicted in the inset of figure 1. The metallic core shows a bulk-like FeCo crystal lattice as reported in [26]. EDX yields a stoichiometry of Fe: (56 ± 5)% and Co: (44 ± 4)% being close to the target composition similar to previous investigations. The oxide thickness is estimated to about (2.0 ± 0.5) nm analogously to respective findings on Fe and Co nanoparticles [28, 29]. Based on the thickness and atomic density of bulk-like $CoFe_2O_4$ we obtain the distribution of the particle sizes *before oxidation* as given in figure 1. The TEM grids used in this work are covered with an amorphous carbon layer. Thus, we suppose that the mean diameter of (10.0 ± 1.5) nm corresponds to the original particles in the cluster beam. The shape of free nanoparticles in thermal equilibrium is determined by the surface facet energies according to the Wulff theorem [30, 31]. For bcc Fe particles truncated dodecahedrons with (001) and (110) facets have been found experimentally [26, 29]. Assuming comparable energies for the corresponding surfaces the same shape is expected for FeCo nanoparticles (possessing a CsCl-type crystal lattice) in the given size regime.

3.2. STM investigations on FeCo nanoparticles on W(110)

FeCo particles of the same size are deposited onto W(110) and studied *in situ* by scanning tunneling microscopy. The STM image displayed in the inset of figure 2 shows a random distribution of the nanoparticles over the terraces. A preferential deposition site at steps with atomic height or agglomeration does not occur. This observation is in accordance with the anticipated vanishing mobility of clusters in strongly interacting metal-on-metal systems at room temperature and has also been observed in other experiments, cf e.g. [32, 33]. A high resolution image of an individual particle is given in figure 3. The apparent shape is governed by particle-tip convolution. Successful shape reconstruction has been reported before, whereas the result of respective approaches depends on several factors such as, for example,

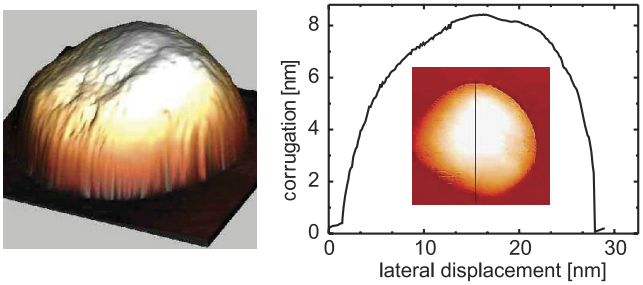

Figure 3. Left: STM image of an individual cluster from figure 2. Image size is 32 nm × 32 nm, $I = 0.1$ nA, $U = +1.0$ V. Right: corresponding corrugation, the height (see the line section in the inset) is determined to be about 8.5 nm.

tip shape stability during the experiment, cf [34]. However, the height of the particle can unambiguously be determined to about 8.5 nm (cf the right panel of figure 3)[5]. The observed particle heights (see figure 2) vary between 7 and 12 nm with an averaged height of $h = (8.7 \pm 1.3)$ nm. When compared to the diameters determined from the TEM images (figure 1), the particles thus appear partially flattened on the W(110) surface. Assuming a constant volume before and after deposition and a shape of a spherical cap the corresponding particle (lateral maximum) width amounts to $w = (10.2 \pm 2.0)$ nm, yielding an aspect ratio $a = h/w$ of 0.85 ± 0.21.

Flattening of supported nanostructures in thermal equilibrium has been observed in several experiments and its magnitude depends on the surface energy γ_{NP} of the nanoparticle and the adhesion energy E_{adh} required to remove the particle from the support [36, 37]. The Wulff–Kaischew theorem predicts partial flattening for $E_{\mathrm{adh}} > \gamma_{\mathrm{NP}}$ and fully two-dimensional wetting for $E_{\mathrm{adh}} > 2 \cdot \gamma_{\mathrm{NP}}$ [38]. In molecular

[5] In [35], it has been reported that the height of smaller nanoparticles as determined by STM depends to a certain extent on the applied tunneling voltage. In particular, gold particles with diameters of about 2.4 nm have shown an apparent size reduction of about 20% when applying a comparably large voltage of +3.5 V. In the present experiments a tunneling voltage of $U = +1.0$ V has been applied. Furthermore, the tip–particle distance (∼1 nm) here is much smaller than the particle diameter. Thus, we suppose that our height determination is not significantly distorted by these effects.

beam epitaxy experiments on Fe and Co on W(110) a distinct surface wetting has been observed. This is ascribed to the high surface energy of 4 J m^{-2} for W(110) relative to iron and cobalt (about 2.4 J m^{-2} [39, 40]). For low coverages the thermal equilibrium state is given by the formation of pseudomorphic islands with monoatomic height in both cases. In the current studies, on the other hand, preformed particles are softly deposited. They retain a 3D shape, obviously of metastable character, where the transition to thermal equilibrium is kinetically hindered. Homoepitaxy experiments on iron reveal diffusion constants of about 10^3 nm^2 s^{-1} at room temperature [41]. Thus, diffusion of surface atoms being released from their binding sites might provide an effective material transport channel for nanoparticles. However, the energy required to remove an atom from a closed surface facet of a nanoparticle (of the order of ∼1 eV) is much higher than the thermal energy at room temperature and the probability of a diffusion event is severely limited. As a consequence the particles remain stable during the present STM experiments (several hours) and we conclude that the observed partial flattening occurs immediately upon the impact on the substrate. At higher temperatures the transition from larger iron and cobalt islands to flat layers on W(110) can be driven on a timescale of several minutes [42].

3.3. Magnetization curves of Fe clusters on W(110)

The impact of partial flattening on the magnetic anisotropy of supported nanostructures is studied with Fe nanoparticles with similar diameters $D = (9.6 \pm 1.5)$ nm. For spherical systems of this size, a blocking temperature of ∼110 K is expected, assuming the magneto-crystalline bulk MAE [43]. Without other effects this would result in an isotropic and superparamagnetic behavior of a respective nanoparticle ensemble at room temperature. However, experimental magnetization curves of the Fe nanoparticles on W(110) reveal a distinct magnetic anisotropy with preferred in-plane orientation of the magnetic moments. This is shown in figure 4 where the black circles (open red circles) correspond to the magnetization measured with the magnetic field applied parallel (perpendicular) to the sample surface. The particle density of the sample is about 200 μm^{-2}. Calculations show that dipolar interactions in such an ensemble can be neglected: thus we ascribe the observed magnetization curves to the magnetic anisotropy of the individual nanoparticles. A corresponding equation describing magnetization curves of superparamagnetic nanoparticles in the presence of an additional uniaxial anisotropy term has been derived in [6]. Based on this, an uniaxial anisotropy constant $K = (5.7 \pm 1.7)$ μeV/atom can be obtained from a fit to the present data (solid lines). This value is larger than the Fe bulk anisotropy of 3.3 μeV/atom [51], but much smaller when compared to prominent high anisotropy systems as small Co clusters and atomic chains on Pt(111) with a MAE of the order of 1 meV/atom [6]. For the fit in figure 4 it is assumed that the surface normal represents a magnetic hard axis while all in-plane directions are equally preferred. An additionally possible in-plane anisotropy is neglected as discussed further below.

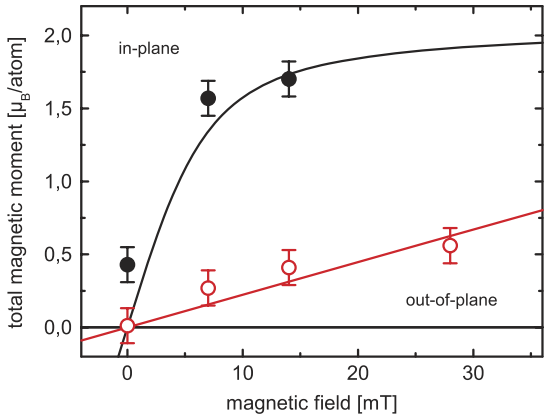

Figure 4. Magnetization of (9.6 ± 1.5) nm Fe clusters on W(110) with the magnetic field applied in the surface plane (full symbols) and out-of-plane (open symbols) as measured at room temperature. The solid lines are fits to the data according to [6].

The average number of atoms in the Fe nanoparticles has been set to $N = 52\,500$ atoms according to their mean size and the magnetic moment is equal to $\mu = 2.1\ \mu_B$/atom, the bulk value of bcc Fe at room temperature. Note that, based on the obtained anisotropy constant, the total MAE per particle is about 300 meV and thus much larger than the thermal energy at room temperature. Nevertheless, the particles still remain superparamagnetic, but with the magnetization preferentially fluctuating in the sample plane.

3.4. Magnetic anisotropy energy of supported Fe nanoparticles

The total magnetic anisotropy energy of supported nanoparticles is determined by shape, surface, interface and magneto-crystalline contributions. For a more precise analysis, strain-induced magneto-elastic modifications of each contribution also have to be taken into account [44]. However, lacking reliable information on the strain profile in the particles only bulk-like properties are considered here. Shape and interface contributions are governed by the overall particle geometry while the interface contribution is determined by the number of contact atoms to the substrate. When varying the particle shape, generally both terms are affected. In order to gain more insight into the relative influence of the different contributions we calculate the respective anisotropy energies based on atomically modeled nanoparticles. The starting point for deriving respective models is the 'free' nanoparticle as given by the Wulff theorem. The best approximation to the present particle size consists of 52 759 atoms and shows 6 (001) and 12 (110) facets. The height and width of the particle is 9.76 nm, while the aspect ratio is 1.0. A sketch of the particle is depicted (denoted as Wulff NP) in the inset of figure 5. By adding and removing (001) and (110) surface planes while keeping the number of atoms (almost) constant we alter the particle shape covering aspect ratios from 0.8 to 1.0. For $a = 0.8$ we obtain $N = 52\,761$ with $h = 8.18$ nm and $w = 10.33$ nm, cf inset (flatt. NP) in figure 5. For simplicity we assume that the particles rest with a (001) facet on the substrate surface.

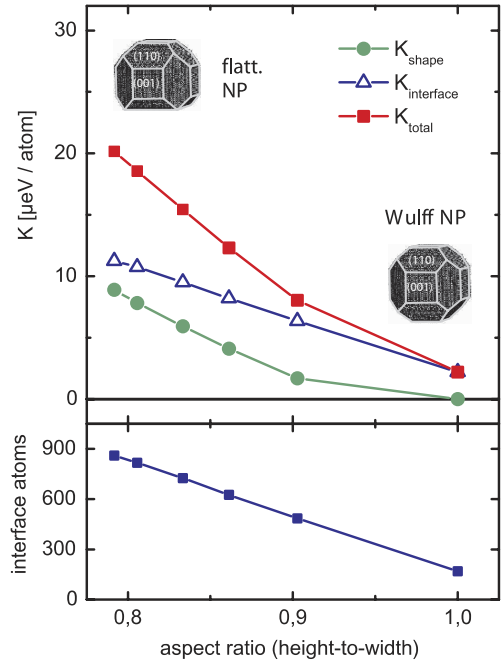

Figure 5. Top: calculated shape, interface and total anisotropy energy constants. The insets depict the highly symmetric Wulff nanoparticle ($a = 1.0$) and a flattened particle with $a = 0.8$. Bottom: number of interface atoms sitting on the (100) contact facet.

The shape anisotropy energy results from the demagnetizing stray field and is thus determined by the particle geometry. Assuming a collinear spin configuration and constant magnetic moments (2.1 μ_B/atom), the shape anisotropy constant K_{shape} is calculated by summation of the dipolar interactions over the whole particle: for details see, e.g., [45]. The Wulff nanoparticle is highly symmetric and thus shows no shape anisotropy. Altering the particle shape results in a noticeable rise of K_{shape} as shown by the full circles in the upper panel of figure 5. The considered particle models are symmetric with respect to the surface normal and exhibit no additional in-plane anisotropy. Therefore, the calculated values of K_{shape} correspond to a uniaxial anisotropy with the magnetic hard axis being perpendicular to the sample surface. For aspect ratios close to the experimentally observed value of 0.85 (cf section 3.2) the calculations yield a shape anisotropy energy of about 5 μeV/atom, being in good agreement with the value obtained from the measured magnetization curves.

The surface anisotropy originates from the broken crystal lattice symmetry at the particle surface and can be calculated by summation of magnetic pair interactions of the form $L\cos^2(\theta)$, with θ being the angle between the intersection line of two adjacent atoms and the magnetic moment, and L the material-dependent Néel constant [46]. Similarly to the shape anisotropy, it vanishes in the case of the highly symmetric Wulff nanoparticle. Using $L = -112$ μeV/atom [45] it turns out that the surface anisotropy contribution is also negligible for all other particles under consideration due to the comparably small surface-to-volume ratio in the present size regime.

Instead, a significant contribution to the MAE results from the interface to the substrate. For Fe films on W(110), a remarkably strong interface anisotropy with preferred in-plane magnetization due to strain and electronic hybridization effects is well known [47–49]. The actual film thickness dependence of the anisotropy energy is governed by the competition of interface, strain and shape contributions [50]. For the present discussion we rely on the anisotropy energy per interface atom that has been estimated in [48]. The corresponding out-of-plane anisotropy energy amounts to +0.69 meV per interface atom. A comparably weak in-plane anisotropy of +0.12 meV is also found but neglected in the following. The resulting $K_{interface}$ of the supported nanoparticles is calculated based on the number of interface atoms. For the unflattened Wulff particle we find $K_{interface} = 2.2$ μeV/atom. As shown by the open triangles in figure 5 the interface anisotropy increases with the number of contact atoms (given in the lower panel of figure 5) and is always larger than the respective shape contribution in the present aspect ratio range. Since both anisotropies act similarly on the magnetization, they add up and yield K_{total} as given by the closed squares in the figure. Based on these values we find that an aspect ratio of about 0.95 is required to explain the experimentally observed anisotropy. Since it is unclear whether the interface anisotropy of deposited nanoparticles has the same magnitude when compared to that of epitaxially grown iron films on W(110) we suppose that this value presents an upper limit and smaller aspect ratios might be required.

Finally, we consider the magneto-crystalline anisotropy resulting from coupling of the spins to the crystal lattice via spin–orbit interaction. In the case of bcc Fe it represents a fourth-order contribution with a magnitude of 3.3 μeV/atom (at room temperature [51]) to the total MAE with the magnetic easy axes along the (001) directions. Its influence on the magnetization curve depends crucially on the distribution of the nanoparticle crystal axes in the ensemble under investigation. In contrast to the shape and interface anisotropy (which rely solely on the presence of a supporting interface) a random orientation of the crystal axes upon deposition would result in isotropic magnetic properties of a respective particle ensemble. In this case the uniaxial contribution may then dominate the magnetization curves. An identical orientation of the particles would change the situation but experimental evidence for an alignment to the substrate lattice upon deposition is not yet available. Nevertheless, based on the data in figure 5, we conclude that the uniaxial shape and interface contributions become dominant for aspect ratios being smaller than about 0.85, independent of the actual particle orientation.

4. Conclusion

Mass-filtered pure Fe and FeCo alloy nanoparticles with a diameter of about 10 nm are deposited under soft-landing and UHV conditions onto a bare W(110) surface. The structure and the stoichiometry of the FeCo alloy nanoparticles are determined by *ex situ* HRTEM and EDX on individual nanoparticles proving a crystalline structure. *In situ* STM experiments show that the nanoparticles deposited from the arc cluster ion source are irregularly distributed on the W(110)

surface, that no fragmentation occurs, that atomic steps do not act as preferential adsorption sites, and that a noticeable interaction with the substrate is present which leads to a flattening of the deposited clusters upon deposition. The resulting height-to-width aspect ratio is about 0.85. The impact of partial flattening on the magnetic anisotropy is studied based on pure Fe nanoparticles on W(110). Angular-dependent magnetization measurements reveal an uniaxial magnetic anisotropy with the magnetic hard axis being perpendicular to the surface plane. This finding is discussed with respect to shape anisotropy as well as to the strong interface anisotropy being known from iron films epitaxially grown on W(110). Comparing the experimentally obtained anisotropy energy with respective calculations shows that partial flattening with an aspect ratio of less than 0.94 may explain the experimental magnetization curves depending on the magnitude of the interface energy. The surface anisotropy is negligible in the present size range. The actual contribution of the magneto-crystalline anisotropy to the total MAE remains open without further information on the particle alignment.

Acknowledgments

We would like to thank M Spasova (University of Duisburg–Essen) for taking the TEM pictures. Furthermore, we are in debt to V von Oeynhausen and I Barke (University of Rostock) for fruitful discussions. We gratefully acknowledge technical support by the staff of BESSY in Berlin, and financial support by the Deutsche Forschungsgemeinschaft (DFG) within the priority program 1153 'Clusters in Contact with Surfaces' (project nos. GE 1026/4-2, KL 2188/1-3, BA 1612/3-2 and-3).

References

[1] Haberland H 1995 *Clusters of Atoms and Molecules* (Berlin: Springer)
[2] Meiwes-Broer K H 2000 *Clusters on Surfaces* (Berlin: Springer)
[3] Bansmann J *et al* 2005 *Surf. Sci. Rep.* **56** 189
[4] Billas I M L, Châtelain A and de Heer W A 1994 *Science* **265** 1682
[5] Bucher J P, Douglass D C and Bloomfield L A 1991 *Phys. Rev. Lett.* **66** 3052
[6] Gambardella P *et al* 2003 *Science* **300** 1130
[7] Lau J T, Föhlisch A, Nietubyć R, Reif M and Wurth W 2002 *Phys. Rev. Lett.* **89** 057201
[8] Edmonds K W, Binns C, Baker S H, Thornton S C, Norris C, Goedkoop J B, Finazzi M and Brookes N B 1999 *Phys. Rev.* B **60** 472
[9] Guirado-López R A, Dorantes-Dávila J and Pastor G M 2003 *Phys. Rev. Lett.* **90** 226402
[10] Bartolomé J *et al* 2008 *Phys. Rev.* B **77** 184420
[11] Luis F *et al* 2006 *Europhys. Lett.* **76** 142
[12] Pierce J P, Torija M A, Gai Z, Shi J, Schulthess T C, Farnan G A, Wendelken J F, Plummer E W and Shen J 2004 *Phys. Rev. Lett.* **92** 237201
[13] Bansmann J, Getzlaff M, Kleibert A, Bulut F, Gebhardt R K and Meiwes-Broer K H 2006 *Appl. Phys.* A **82** 73
[14] Bansmann J and Kleibert A 2005 *Appl. Phys.* A **80** 957
[15] Huber D L 2005 *Small* **1** 482
[16] Sun S, Murray C B, Weller D, Folks L and Moser A 2000 *Science* **287** 1989
[17] Ethirajan A *et al* 2007 *Adv. Mater.* **19** 406
[18] Wiedwald U, Klimmer A, Kern B, Han L, Boyen H G, Ziemann P and Fauth K 2007 *Appl. Phys. Lett.* **90** 062508
[19] Burkert T, Nordström L, Eriksson O and Heinonen O 2004 *Phys. Rev. Lett.* **93** 027203
[20] Andersson G *et al* 2006 *Phys. Rev. Lett.* **96** 037205
[21] Stöhr J and König H 1995 *Phys. Rev. Lett.* **75** 3748
[22] Chen C T, Idzerda Y U, Lin H J, Smith N V, Meigs G, Chaban E, Ho G H, Pellegrin E and Sette F 1995 *Phys. Rev. Lett.* **75** 152
[23] Kortright J B, Awschalon D D, Stöhr J, Bader S D, Idzerda Y U, Parkin S S P, Schuller I K and Siegmann H C 1999 *J. Magn. Magn. Mater.* **207** 7
[24] Joyner R W, Rickman J and Roberts M W 1973 *Surf. Sci.* **39** 445
[25] Methling R P, Senz V, Klinkenberg E D, Diederich Th, Tiggesbäumker J, Holzhüter G, Bansmann J and Meiwes-Broer K H 2001 *Eur. Phys. J.* D **16** 173
[26] Kleibert A, Bansmann J, Passig J, Getzlaff M and Meiwes-Broer K H 2007 *J. Appl. Phys.* **101** 114318
[27] Passig J, Meiwes-Broer K H and Tiggesbäumker J 2006 *Rev. Sci. Instrum.* **77** 093304
[28] Wiedwald U *et al* 2003 *Phys. Rev.* B **68** 064424
[29] Vystavel T, Palasantzas G, Koch S A and De Hosson J Th M 2003 *Appl. Phys. Lett.* **82** 197
[30] Wulff G 1901 *Z. Kristallogr.* **34** 449
[31] Baletto F and Ferrando R 2005 *Rev. Mod. Phys.* **77** 371
[32] Zimmermann C G, Yeadon M, Nordlund K, Gibson J M, Averback R S, Herr U and Samwer K 1999 *Phys. Rev. Lett.* **83** 1163
[33] Bardotti L, Prével B, Mélinon P, Perez A, Hou Q and Hou M 2000 *Phys. Rev.* B **62** 2835
[34] Sell K, Kleibert A, von Oeynhausen V and Meiwes-Broer K H 2007 *Eur. Phys. J.* D **45** 433
[35] Hövel H and Barke I 2006 *Prog. Surf. Sci.* **81** 53
[36] Hansen K H, Worren T, Stempel S, Lægsgaard E, Bäumer M, Freund H J, Besenbacher F and Stensgaard I 1999 *Phys. Rev. Lett.* **83** 4120
[37] Hansen P L, Wagner J B, Helveg S, Rostrup-Nielsen J R, Clausen B S and Topsøe H 2002 *Science* **295** 2053
[38] Henry C R 2005 *Prog. Surf. Sci.* **80** 92
[39] Gradmann U, Liu G, Elmers H J and Przybylski M 1990 *Hyperfine Interact.* **57** 1845
[40] Vitos L, Ruban A V, Skriver H L and Kollár J 1998 *Surf. Sci.* **411** 186
[41] Stroscio J A, Pierce D T and Dragoset R A 1993 *Phys. Rev. Lett.* **70** 3615
[42] Reuter D, Gerth G and Kirschner J 1998 *Phys. Rev.* B **57** 2520
[43] Aharoni A 2000 *Introduction to the Theory of Ferromagnetism* (Oxford: Oxford University Press)
[44] Getzlaff M 2007 *Fundamentals of Magnetism* (Berlin: Springer)
[45] Jamet M, Wernsdorfer W, Thirion C, Dupuis V, Mélinon P, Pérez A and Mailly D 2004 *Phys. Rev.* B **69** 024401
[46] Jamet M, Wernsdorfer W, Thirion C, Mailly D, Dupuis V, Mèlinon P and Pérez A 2001 *Phys. Rev. Lett.* **86** 4676
[47] Gradmann U, Korecki J and Waller G 1986 *Appl. Phys.* A **39** 101
[48] Fritzsche H, Elmers H J and Gradmann U 1994 *J. Magn. Magn. Mater.* **135** 343
[49] Qian X and Hübner W 2001 *Phys. Rev.* B **64** 092402
[50] Elmers H J and Gradmann U 1990 *Appl. Phys.* A **51** 255
[51] Klein H P and Kneller E 1966 *Phys. Rev.* **144** 372